Mon. Not. R. Astron. Soc. **000**, 000–000 (0000) Printed 1 February 2008 (MN LaTeX style file v2.2)

The death of FRII radio sources and their connection with radio relics

Christian R. Kaiser[1]* and Garret Cotter[2]
[1] *Department of Physics & Astronomy, University of Southampton, Southampton SO17 1BJ*
[2] *Cavendish Laboratory, Madingley Road, Cambridge, CB3 0HE*

arXiv:astro-ph/0201288v2 24 Jun 2002

1 February 2008

ABSTRACT
Radio relic sources in galaxy clusters are often described as the remnants of powerful radio galaxies. Here we develop a model for the evolution of such relics after the jets cease to supply energy to the lobes. This includes the treatment of a relic overpressured with respect to its gaseous surroundings even after the jets switch off. We also determine the radio emission of relics for a large variety of assumptions. We take into account the evolution of the strength of the magnetic field during the phase of relativistic particle injection into the lobes. The resulting spectra show mild steepening at around 1 GHz but avoid any exponential spectral cut-offs. The model calculations are used to fit the observed spectra of seven radio relics. The quality of the fits is excellent for *all* models discussed. Unfortunately, this implies that it is virtually impossible to determine any of the important source parameters from the observed radio emission alone.

Key words: galaxies: active – galaxies: jets – intergalactic medium – radio continuum: galaxies

1 INTRODUCTION

Diffuse radio emission without an apparent host galaxy is found in an increasing number of clusters of galaxies (e.g. Giovannini et al., 1999; Giovannini & Feretti, 2000; Kempner & Sarazin, 2001; Govoni et al., 2001). These objects can roughly be divided into radio halos close to the cluster centre which appear comparatively smooth in radio images and radio relics with a far more distorted and knotty appearance. The latter are usually found further away from the central regions (Slee & Reynolds, 1984). Here we concentrate on radio relic sources.

A large number of possible explanations for radio relics has been proposed. All of these aim at explaining the production of a population of relativistic electrons responsible for the observed radio synchrotron emission. The suggested mechanisms range from the turbulent wakes of galaxies moving in the cluster's gravitational potential to cluster mergers. In the present paper we concentrate on the picture of relics as remnants of once powerful radio galaxies or radio-loud quasars. This scenario is based on the idea that the relics are the lobes of former radio galaxies, the jets of which ceased to supply them with energy some time ago (e.g. Komissarov & Gubanov, 1994; Slee et al., 2001). The relativistic electrons, the emission of which we observe today, were accelerated at the strong shocks at the ends of the active jets. The electrons lose their energy due to synchrotron losses, inverse Compton scattering of cosmic microwave background photons and, possibly, further adiabatic expansion of the relics themselves. As the relativistic electrons are not replenished by the active jets, the radiative energy losses introduce a spectral cut-off moving towards low frequencies in time. This can potentially explain the observed steep radio spectra of relics.

Note however that not all relics may be consistent with the picture of the passively fading remnant of a radio galaxy. Some relics are extended and show a rather smooth structure resembling in some ways the appearance of radio haloes, while others are composed of a number of individual knots. The variety of morphologies different from the appearance of active radio galaxies may very well indicate that our interpretation of relics as the remnants of radio galaxies is incorrect in many cases. However, it is not clear what the fate of the material forming the large scale radio structure of a formerly active radio galaxy is. Buoyant rise in the gravitational potential well of the cluster will certainly play a role (e.g. Churazov et al., 2001), but the movement of the parent galaxy through the cluster gas and cluster mergers may fragment the remnant as well. It is therefore not surprising that the morphology of relics is seldomly reminiscent of active radio galaxies. Even if all relics were indeed, as we assume here, the remnants of radio galaxies, the evolution of the remnant may imply significant departures from the simple pressure evolution envisaged in the model introduced here.

Another problem is the possibility of re-acceleration of the relativistic electrons even after the jets have switched off. Slee et al. (2001) present radio observations of the relics in A13, A85, A133 and A4038. The substantial substructure in these sources may well be the signature of some highly dynamic processes being at work which could lead to further acceleration of relativistic particles. In

---

* email: crk@astro.soton.ac.uk

this paper we will neglect any re-acceleration processes which may take place in relics.

The question then is whether or not a passively evolving population of relativistic electrons produces a radio spectrum consistent with observations. The main problem is that the radio spectra of relics are shallow at around 100 MHz and considerably steeper in the GHz; but they do not show exponential cut-offs. The spectra are therefore not consistent with a single population of electrons accelerated all at the same time and passively losing their energy. Taking this extended injection period into account, Komissarov & Gubanov (1994) showed that two breaks appear in the spectrum. The lower break is located at the frequency cut-off of the 'oldest' electrons while the higher break is determined by the 'youngest' electrons. The comparatively mild steepening of the spectra between the breaks is roughly consistent with the observations. Nevertheless, Komissarov & Gubanov (1994) found that for effective pitch-angle scattering of the relativistic electrons the steepening of the spectrum was still too strong. Therefore they had to suppress pitch-angle scattering to further flatten their model spectra.

The exponential cut-off in the spectrum is also avoided in the case of inhomogeneous magnetic field strengths inside the relic. The relativistic electrons spend most of their time in the low-field regions and only occasionally diffuse into the high-field regions. Thus their energy losses are reduced and by careful adjustment of the efficiency of the diffusion process an emission spectrum with mild steepening at high frequencies can be achieved (Tribble, 1994; Eilek et al., 1997). Slee et al. (2001) fitted a model based on this idea to the spectra of relic sources and found good agreement.

Komissarov & Gubanov (1994) assumed that the relics or their progenitors were in pressure equilibrium with their surroundings even at the time of the injection of relativistic electrons. In this paper we expand this model by taking into account the evolution of the lobes during the injection of relativistic particles. If the lobes of radio galaxies of type FRII (Fanaroff & Riley, 1974) are the progenitors of the radio relics, then during the time the jets are still active, the lobes are expanding into the surrounding material. This implies that the pressure inside the lobes and therefore also the strength of the magnetic field are not constant during the particle injection. In fact, the strength of the magnetic field is decreasing and thus relativistic electrons injected at later times can survive for longer. We show that this effect results in radio spectra of the resulting relic sources without exponential cut-offs and a spectral slope comparable to that in observed relics.

At the time the jets switch off, the lobes may still be overpressured with respect to the ambient gas and therefore continue to expand. We derive expressions for the temporal behaviour of the volume and the pressure of such 'coasting' relics. We take such a coasting phase into account in our calculation of model radio spectra from relic sources. Finally, we show that our models fit the observed spectra very well. Unfortunately, we find that none of the important source parameters, like the source age, or the physical processes taking place in the relics can be determined from the radio spectra alone.

In Section 2 we derive the temporal behaviour of a coasting relic source after the jets have switched off. We use the results found to calculate the radio spectra of relic sources in Section 3. Here we also show how the variation of the main model parameters influences the results. In Section 4 we fit the observed spectra of relic sources with our model and show that very little useful information about the conditions in the sources and their environments can be gained from the models. We summarise our results in Section 5.

2 THE SPHERICAL RADIO SOURCE

After the jets of a powerful radio sources switch off, the cocoon inflated during the active phase may still be overpressured with respect to the external medium. It will then enter the 'coasting phase' while continuing to expand behind a strong bow shock. This situation is somewhat reminiscent of the early evolution of a supernova remnant or the explosion of a nuclear weapon. The dynamics of a strong explosion in a uniform atmosphere are described by the similarity solution of Taylor and Sedov (e.g. Sedov, 1959; Landau & Lifshitz, 1987). It is straightforward to generalise this solution for the case of a power-law density distribution in the external medium with $\rho = \rho_0 (r/a_0)^{-\beta}$, where a_0 is the scale height or core radius of the distribution. We will assume this density distribution for all model calculations in this paper. The radius of the spherical bow shock then grows as $R_s \propto t^{2/(5-\beta)}$. Despite the fact that the cocoons of radio galaxies are usually not spherical, one might expect that their expansion during the coasting phase is governed by the same proportionality once the jet activity has ceased. However, in the following we will show that the presence of the contact discontinuity defining the cocoon boundary in radio galaxies requires a different dynamical behaviour.

Goldshmidt & Rephaeli (1994) present a different solution to this problem based on their assumption that the dynamics of the radio source expansion are not influenced by the mass of the external gas swept up by the bow shock. The dynamical behaviour of active radio sources strongly suggests that their cocoons are underdense with respect to the external medium (e.g. Falle, 1991). Therefore it is very unlikely that this assumption can be made for the problem considered here.

2.1 Analytical solutions

For simplicity we will assume that the bow shock and the cocoon are both spherical. In practice both are elongated along the jet axis but this different geometry results only in a change of the constants of proportionality. The dynamical behaviour, i.e. the time dependence of the physical parameters of the flow, will be the same. The cocoon volume is then given by $V_c = 4/3\pi R_c^3$ and that of the layer of shocked gas in between the bow shock and the cocoon is $V_s = 4/3\pi(R_s^3 - R_c^3)$. Furthermore, we also assume that the pressure, p, inside the cocoon and in the shocked layer surrounding it, is uniform. Again, this greatly simplifies the problem and will not change our results apart from the exact numerical values of the normalisations. During the active phase, while the jets are still switched on, conservation of energy for the gas inside V_c requires

$$\frac{4}{3}\pi R_c^3 \dot{p} + 4\pi\gamma_c p R_c^2 \dot{R}_c = (\gamma_c - 1)\, Q_j, \tag{1}$$

where γ_c is the adiabatic index of the cocoon material and Q_j is the energy transport rate of the jets. We will keep Q_j constant during the lifetime of the jets at the end of which it drops to zero instantaneously. Similarly, for the shocked gas inside V_s we find

$$\begin{aligned} \frac{4}{3}\pi\left(R_s^3 - R_c^3\right)\dot{p} \quad &+ \quad 4\pi\gamma_s p\left(R_s^2 \dot{R}_s - R_c^2 \dot{R}_c\right) \\ &= \quad 2\pi\left(\gamma_s - 1\right) R_s^2 \rho_0 \left(\frac{R_s}{a_0}\right)^{-\beta} \dot{R}_s^3, \end{aligned} \tag{2}$$

where γ_s is the adiabatic index of the shocked material. The expression on the right of equation (2) is the rate at which kinetic energy flows into the bow shock (see Kaiser & Alexander, 1997).

Finally, since we consider only strong shocks, the pressure within the source is balanced by the ram pressure of the external medium,

$$p = \rho_0 \left(\frac{R_{\rm s}}{a_0} \right)^{-\beta} \dot{R}_{\rm s}^2 . \tag{3}$$

Equations (1) through (3) are identical to the system of equations studied by Reynolds & Begelman (1997) for the case of intermittent jet sources.

We are interested in steady-state similarity solutions for this set of equations with the three unknown functions $R_{\rm c}$, $R_{\rm s}$ and p being power laws of time. We find

$$\begin{aligned} R_{\rm c} &= \left[\frac{(\gamma_{\rm c}-1)\,(5-\beta)^3}{12\pi\,(9\gamma_{\rm c}-4-\beta)} k^{\frac{\beta-2}{5-\beta}} \right]^{1/3} \left(\frac{Q_{\rm j} t^3}{\rho_0 a_0^{\beta}} \right)^{1/(5-\beta)} \\ R_{\rm s} &= \left(k \frac{Q_{\rm j} t^3}{\rho_0 a_0^{\beta}} \right)^{1/(5-\beta)} \\ p &= \frac{9}{(5-\beta)^2} \left[k^{2-\beta} Q_{\rm j}^{2-\beta} \left(\rho_0 a_0^{\beta} \right)^3 t^{-4-\beta} \right]^{1/(5-\beta)} , \end{aligned} \tag{4}$$

where

$$k = \frac{(\gamma_{\rm c}-1)\,(5-\beta)^3\,(9\gamma_{\rm s}-4-\beta)}{6\pi\,(9\gamma_{\rm c}-4-\beta)\,(9\gamma_{\rm s}+1-2\beta)} . \tag{5}$$

The exponents of the time variable in these equations are equal to those found by Falle (1991) and Kaiser & Alexander (1997) for sources with active jets.

After the jets cease to supply energy to the cocoon, the source enters the coasting phase and we have to set $Q_{\rm j} = 0$. We assume that the cocoon stays overpressured with respect to the surrounding medium. In this case, equation (1) describes the now adiabatic expansion of the cocoon, i.e. $p \propto R_{\rm c}^{-3\gamma_{\rm c}}$. With this, equations (2) and (3) in principle again yield power-law similarity solutions with $R_{\rm c} \propto R_{\rm s} \propto t^{2/(2-\beta+3\gamma_{\rm c})}$. Note that this is different from the Taylor-Sedov solution. This difference is caused by the adiabatic behaviour of the cocoon driving the bow shock for which there is no analogon in the case of a strong explosion. The ratio of the radius of the spherical cocoon and the bow shock is given by

$$\frac{R_{\rm c}}{R_{\rm s}} = \left[1 - \frac{\gamma_{\rm s}-1}{2\,(\gamma_{\rm s}-\gamma_{\rm c})} \right]^{1/3} . \tag{6}$$

Obviously, this solution cannot be correct for $\gamma_{\rm c} = \gamma_{\rm s}$ or $\gamma_{\rm s} = 2\gamma_{\rm c} - 1$ which includes the case of a relativistic cocoon ($\gamma_{\rm c} = 4/3$) surrounded by 'cold' material ($\gamma_{\rm s} = 5/3$). Nevertheless, we will see in section 2.2 that in the latter scenario the steady-state solution is an excellent approximation to the evolution of $R_{\rm c}$.

For $\gamma_{\rm c} = \gamma_{\rm s}$ all terms containing $R_{\rm c}$ in equation (2) cancel and a different steady-state solution is possible with

$$\begin{aligned} R_{\rm c} &\propto t^{\frac{2(\gamma_{\rm c}+1)}{\gamma_{\rm c}(7+3\gamma_{\rm c}-2\beta)}} \\ R_{\rm s} &\propto t^{\frac{4}{7+3\gamma_{\rm c}-2\beta}} \\ p &\propto t^{\frac{-6(\gamma_{\rm c}+1)}{7+3\gamma_{\rm c}-2\beta}} . \end{aligned} \tag{7}$$

This implies that the ratio $R_{\rm c}/R_{\rm s}$ is no longer a constant. Despite this, the expansion of the bow shock and that of the cocoon are still intrinsically self-similar.

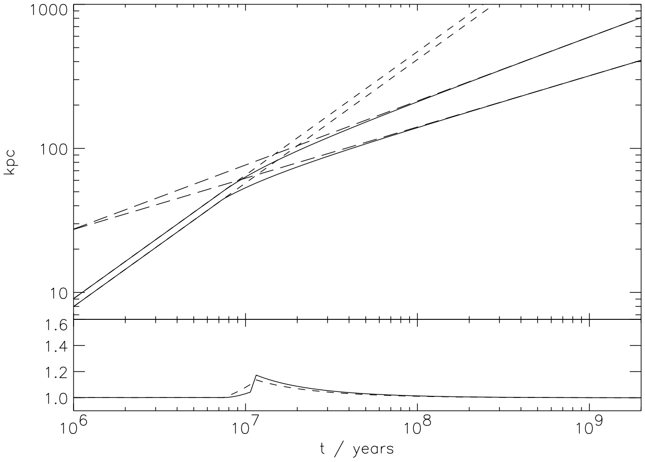

Figure 1. Comparison of the numerical results with the analytical solutions for $\gamma_{\rm c} = \gamma_{\rm s} = 5/3$. Upper panel, solid lines: Numerical results for $R_{\rm c}$ (lower line) and $R_{\rm s}$ (upper line); short dashed lines: analytical solution for active jets; long dashed lines: analytical solutions for 'coasting phase'. Lower panel: Analytical solutions divided by numerical solutions. Dashed line: Ratio for $R_{\rm c}$, solid line: Ratio for $R_{\rm s}$.

2.2 Numerical solutions

All of the solutions derived in the previous section describe steady-state configurations. To assess how quickly a spherical radio source would change from one of these states to another when the jets are switched off, we also integrated the equations (1) to (3) numerically. For this we set $Q_{\rm j} = 10^{46}\,{\rm ergs\,s^{-1}}$, $\rho_0 = 1.7 \times 10^{-25}\,{\rm g\,cm^{-3}}$, $a_0 = 500\,{\rm pc}$ and $\beta = 1.5$. The same values were used by Reynolds & Begelman (1997) and they imply that $\rho_0 a_0^{\beta} = 10^7\,{\rm g\,cm^{-1.5}}$. At a source lifetime of 10^7 years, we 'switched off' the jets by setting $Q_{\rm j} = 0$. For the integration we used a standard Runge-Kutta algorithm. The initial conditions were derived from equations (4).

Figure 1 shows the results of this numerical integration for the radius of the bow shock, $R_{\rm s}$, and that of the cocoon, $R_{\rm c}$ for the case $\gamma_{\rm c} = \gamma_{\rm s} = 5/3$. The analytical solutions for the still active jets are calculated from equations (4). For the coasting phase we used equations (7). Here we are free to choose the normalisation of the analytical solutions as these are not constrained by the equations. We have chosen the normalisation such that the analytical solution agrees with the numerical results at 2×10^9 years. The lower panel of Figure 1 shows the ratio of the analytical solutions and the numerical results. We have used the analytical solutions for the active phase for times less than 10^7 years and those for the coasting phase for later times. The discrepancy between the two solutions is always less than 20%.

Figure 2 compares the numerical results for the case $\gamma_{\rm c} = 4/3$ and $\gamma_{\rm s} = 5/3$ with the steady-state similarity solutions. As expected, the agreement is worse. Particularly the radius of the bow shock grows more quickly than predicted by the power-law solution. However, the radius of the cocoon is still well described by the steady-state solution. The disagreement between the numerical integration and the analytical power-law is comparable for this case to that for $\gamma_{\rm c} = \gamma_{\rm s}$. We therefore conclude that the dynamical behaviour of the cocoon of a spherical radio source adjusts quickly to the cessation of the energy supply by the jets.

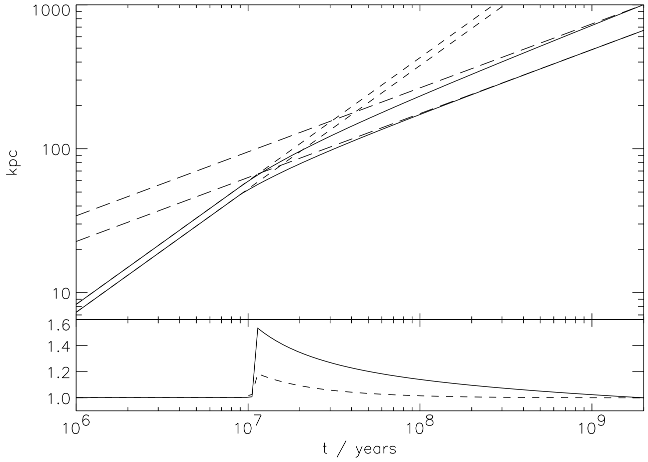

Figure 2. Same as figure 1 but with $\gamma_{\rm c} = 4/3$ and $\gamma_{\rm s} = 5/3$.

2.3 Application to 'real' radio sources

The cocoons of radio sources are elongated along the jet axis. Because of the different external density the various source parts are immersed in, this deviation from purely spherical shape may lead to a different dynamical behaviour at the tip of the cocoon compared to its base. In steady-state this adds only numerical factors to the solutions discussed above. However, it may prolong the transition to the coasting phase at the end of the lifetime of the jets. To investigate this possibility, fully 3-dimensional simulations of radio sources making the transition from active to coasting are needed (e.g. Reynolds, Heinz & Begelman, 2001). To date the evidence from these simulations is somewhat inconclusive. Nevertheless, it is unlikely that the geometrical shape of the radio source strongly influences its evolutionary behaviour.

So far we have implicitly assumed that the information that the jets have ceased to supply energy to the cocoon propagates instantaneously through the whole cocoon. This is a good approximation if the cocoon is small and the internal sound speed is very high. Kaiser & Alexander (1997) show that in the absence of significant mixing of the cocoon material with the surrounding gas across the cocoon boundary the internal sound speed is indeed high. In cases where mixing is important, the sound travel time along the cocoon may become comparable to or even exceed the dynamical timescale. Most of the cocoon will then continue for a significant time to expand as if it was still in the active phase (e.g. Kaiser, Schoenmakers & Röttgering, 2000).

In any scenario the pressure in the cocoon will eventually become comparable to the thermal pressure of the surrounding gas. At this point, the expansion will slow down and the bow shock weakens. Once pressure equilibrium is reached, the expansion stops altogether and the pressure does not change anymore. When exactly this happens depends on the temperature of the external gas. Again the transition of the cocoon from expansion to pressure equilibrium will be a gradual process with those regions of the cocoon close to the centre of the density distribution coming into pressure equilibrium first (e.g. Baldwin, 1982). Even in this equilibrium phase the cocoon will not be static. As it is underdense with respect to the surrounding gas it will start rising due to buoyancy (e.g. Gull & Northover, 1973; Churazov et al., 2001; Brüggen & Kaiser, 2001) and the pressure inside the cocoon is decreasing. However, the timescale for this rise usually exceeds the lifetime of the relativistic electrons. The equilibrium phase was also considered by Komissarov & Gubanov (1994). For simplicity we study in this paper the case of a radio source which comes into pressure equilibrium with its surroundings at the same time as the jets switch off. We will also assume that the transition is instantaneous and that the pressure within the cocoon is uniform.

In the following study of the radio emission from coasting or equilibrium radio sources we will concentrate on three limiting cases. In each case the jets stop to supply energy to the cocoon at time $t_{\rm s} < t$, where t is the time of observation.

Model A: The internal sound speed is slow and so the cocoon continues to evolve as if the jets were still supplying it with energy, i.e. $R_{\rm c} \propto t^{3/(5-\beta)}$ and $p \propto t^{(-4-\beta)/(5-\beta)}$ even for $t > t_{\rm s}$.

Model B: The internal sound speed is fast and so the cocoon immediately changes from the active phase to the coasting phase, i.e. for $\gamma_{\rm c} = \gamma_{\rm s} = 5/3$ and $t > t_{\rm s}$ we use equations (7).

Model C: The source is in pressure equilibrium with its surroundings from the time $t_{\rm s}$. In this case $R_{\rm c}$ and p are both constants between $t_{\rm s}$ and t.

3 RADIO EMISSION FROM AN INACTIVE RADIO SOURCE

The relativistic electrons responsible for the emission of radio synchrotron emission are accelerated by the shocks at the end of the active jets and injected into the cocoon. They subsequently loose their energy due to adiabatic expansion of the cocoon, synchrotron radiation and inverse Compton scattering of CMB photons. All these processes are cumulative and so relativistic electrons injected into the cocoon later may still radiate while material injected earlier may have faded already. The model of Kaiser, Dennett-Thorpe & Alexander (1997) for active sources allows to track the evolution of the energy distribution of the relativistic electrons injected at a given time $t_{\rm i}$. The total radio spectrum is then found by integrating up the contributions of all electrons injected into the cocoon between $t_{\rm i} = 0$ and $t_{\rm i} = t$, where t is the current age of the source. In the following we will use this model with the modifications detailed in Kaiser (2000) also for the calculation of the emission of sources in the coasting phase.

The model employed relies on all relevant physical quantities having power-law dependencies on time. We have seen in the previous sections that this is, at least approximately, the case for the coasting phase. We find the total radio emission of the cocoon for Model A by simply setting the upper limit of the integration over $t_{\rm i}$ to $t_{\rm s} < t$ at which the jets switched off. In addition, for Models B and C we have to slightly modify the basic approach of Kaiser et al. (1997). The relativistic electrons injected into the cocoon at time $t_{\rm i}$ during a short time interval $\delta t_{\rm i}$ are contained in a volume δV. To determine the radio synchrotron emission from δV, we need to know the energy distribution of the relativistic electrons and the energy density of the magnetic field inside δV. These are completely determined by the evolution of δV and the pressure, p, as functions of time. Defining $\delta V_{\rm s} = \delta V\left(t_{\rm s}\right)$ and $p_{\rm s} = p\left(t_{\rm s}\right)$, yields for Model B at $t > t_{\rm s}$

$$\delta V = \delta V_{\rm s} \left(\frac{t}{t_{\rm s}}\right)^{\frac{6(\gamma_{\rm c}+1)}{\gamma_{\rm c}(7+3\gamma_{\rm c}-2\beta)}} \text{ and } p = p_{\rm s} \left(\frac{t}{t_{\rm s}}\right)^{\frac{6(\gamma_{\rm c}+1)}{7+3\gamma_{\rm c}-2\beta}}, \qquad (8)$$

where we have assumed that each volume element δV undergoes adiabatic expansion with $\delta V \propto R_{\rm c}^3$. This follows naturally as the sum of all volume elements δV must be equal to the total volume of the cocoon. The time dependencies are then given by equations

Table 1. Model parameters for the fiducial model (see text).

fixed parameters	$R_{\rm T}$	2
	s	2.5
	$\gamma_{\rm max}$	10^6
	β	1.5
	z	0.1
free parameters	t / years	10^8
	$t_{\rm s}$ / years	10^8
	$p_{\rm s}$ / ergs cm^{-3}	3×10^{-13}
derived parameters	$Q_{\rm j}$ / ergs s^{-1}	10^{46}
	$\rho_0 a_0^{\beta}$ / g cm$^{-1.5}$	10^7

(7). Obviously, for Model C we have $\delta V = \delta V_{\rm s}$ and $p = p_{\rm s}$ for all times $t > t_{\rm s}$. With this it is now straightforward to compute the synchrotron emission of each δV and numerically integrate over the injection time $t_{\rm i}$ as described in Kaiser et al. (1997).

Kaiser et al. (1997) assume efficient pitch-angle scattering for the relativistic electrons moving in the magnetic field. This is usually referred to as JP-type models (Jaffe & Perola, 1973). For inefficient scattering, the electrons with large pitch-angles, θ, loose their energy faster than those with small θ (KP-type models: Kardashev, 1962; Pacholczyk, 1970). It is straightforward to modify the present model to account for negligible pitch-angle scattering by assuming a uniform pitch-angle distribution and the introduction of one further integral over θ. We calculate the radio emission from all models with and without pitch-angle scattering.

The model for the radio emission depends on the following parameters (see also Kaiser et al., 1997; Kaiser, 2000): t the current age of the source, $t_{\rm s}$ the time at which the jets switched off, $p_{\rm s}$, the pressure in the cocoon at $t_{\rm s}$, $R_{\rm T}$, the aspect ratio of the cocoon, s, the exponent of the initial power-law energy distribution of the relativistic electrons, $\gamma_{\rm max}$, the high energy cut-off of this distribution, β, the exponent of the density distribution of the external medium and, z, the cosmological redshift of the source. Kaiser (2000) shows that most of these parameters are degenerate in the sense that their values do not determine the shape of the radio spectrum in a unique way. We therefore concentrate on the effects of changing $p_{\rm s}$, t and $t_{\rm s}$ and keep all other parameters fixed at their fiducial values given in table 1. We also assume that, at least at the time of injection into the cocoon, the magnetic field is in equipartition with the relativistic particles in each δV. We neglect any contribution to the cocoon pressure from non-radiating particles, i.e. thermal electrons or protons. With these assumptions and free parameters a model spectrum is completely determined except for a multiplicative normalisation constant, $A_{\rm f}$. For the fiducial model we set $A_{\rm f} = 1$. From $p_{\rm s}$, $t_{\rm s}$ and $A_{\rm f}$ it is possible to infer the energy transport rate of the jets, $Q_{\rm j}$, and $\rho_0 a_0^{\beta}$, which describes the density distribution of the gas surrounding the source (see Kaiser, 2000, for details).

For the fiducial model as described in table 1, $t = t_{\rm s}$ and so the jets are still active. The curves labeled 'f' in Figure 3 show the spectrum for this model with (JP) and without (KP) pitch-angle scattering. With an age of 10^8 years, the fiducial model predicts a fairly aged synchrotron spectrum. However, the cumulative energy losses of the relativistic electrons due to synchrotron radiation and inverse Compton scattering are more severe at high frequency for the JP-type model. The other model spectra in Figure 3 are for the same model parameters as the fiducial model but with an age $t = 2 \times 10^8$ years which implies a coasting phase of 10^8 years after $t_{\rm s}$. The spectral shape is very similar among all JP-type and KP-type models so that they appear to be the same spectrum simply shifted along the two coordinate axes. This is caused by the, for the chosen parameters, rather weak energy losses of the relativistic electrons after $t_{\rm s}$. The break in the energy distribution of these electrons is set mainly by the losses before $t_{\rm s}$ and so occurs at roughly the same energy in all models. The break in the spectrum resulting from this is then simply shifted in frequency/flux space by the strength of the magnetic field. Since the energy density of the magnetic field is proportional to the pressure in the cocoon, it follows from Section 2 that models A and C should have the lowest and highest break frequency respectively. This is confirmed by Figure 3. Note here that for our choice of $\gamma_{\rm c}$ and β the behaviour of p as a function of time for models A ($p \propto t^{-11/7}$) and B ($p \propto t^{-16/9}$) is very similar, even for cases with larger energy losses of the relativistic electrons. In fact, usually $0 \leq \beta \leq 2$ and as long as $\gamma_{\rm c} = 5/3$, Models A and B are always similar. As expected, the spectral break occurs at higher frequencies for the KP-type models compared to the JP-type models.

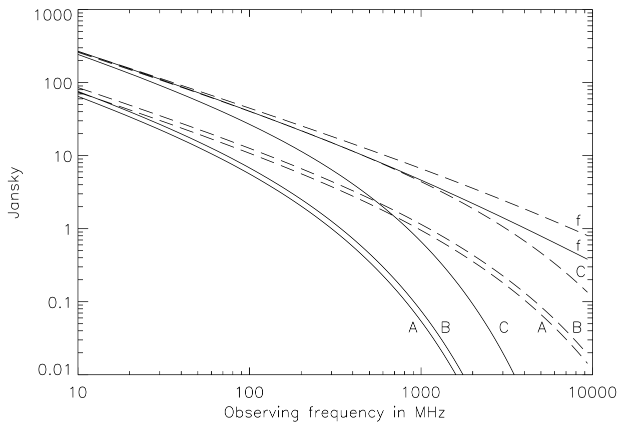

Figure 3. Model results for various coasting radio sources. Solid lines: With efficient pitch-angle scattering, dashed lines: Without pitch-angle scattering. Labels refer to the various models defined in the text. 'f' is the fiducial model and curves labeled 'A', 'B' and 'C' are for the same source but with $t = 2 \times 10^8$ years.

Figure 4 shows a comparison of the effects of varying the free parameters t, $t_{\rm s}$ and $p_{\rm s}$. For this comparison we use the fiducial Model A with effective pitch-angle scattering and $t = 2 \times 10^8$ years. Since the energy densities of the magnetic field and that of the relativistic electrons is proportional to the pressure in the cocoon, an increased $p_{\rm s}$ results in a higher radio flux at low frequencies. However, the energy losses of the particles due to synchrotron emission are also increased moving the break in the spectrum to lower frequencies. Keeping the ratio $t_{\rm s}/t$ constant but decreasing the source age to $t = 10^7$ years, results in a brighter source at low frequencies with the spectral break moving to higher frequencies. At low frequencies the younger age implies a higher cocoon pressure which leads to an increased radio flux. As the radiative energy losses of the relativistic electrons are cumulative, the younger source age simply translates to smaller total losses and therefore a higher break frequency.

Finally we note here that the injection of the relativistic electrons by the jets into the cocoon over a range of time leads to a flatter spectrum at high frequencies than for a single burst injection (e.g. Leahy, 1991). 'Mild' breaks observed in the spectra of radio sources are often interpreted, when using single burst injection

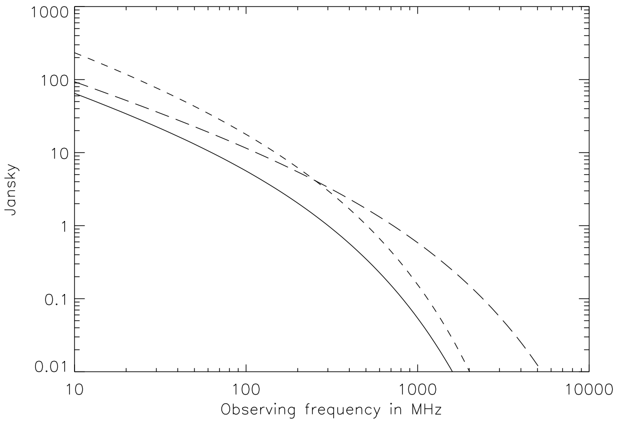

Figure 4. Model results for varying model parameters. Solid curve: Model A for fiducial parameters but with $t = 2 \times 10^8$ years and efficient pitch-angle scattering (same as solid line labeled 'A' in Figure 3). Short-dashed curve: Same model but with $p_\mathrm{s} = 1.5 \times 10^{-12}$. Long-dashed curve: Same model but with $t = 2 \times 10^7$ years and $t_\mathrm{s} = 10^7$ years.

models (as assumed in Komissarov & Gubanov, 1994), as resulting from the suppression of pitch-angle scattering. For a range in the injection time, a similar flattening may be achieved even for efficient pitch-angle scattering.

4 COMPARISON WITH THE SPECTRA OF RADIO RELICS

In this section we will use the models developed above to fit the observed spectra of radio relic sources. In order to compare our results with those of Komissarov & Gubanov (1994), we use their data points and error estimates for the same relic sources, i.e. Mol 0100-22 (or MRC 0100-221), Cul 0038-096, 4C 38.39, 4C 63.10, 3C 318 and 3C 464. The names of the clusters these sources are found in is given in table 2. As discussed in Komissarov & Gubanov (1994), there is a contradiction between the flux measurements of Slee & Reynolds (1984) and Slee, Perley & Siegman (1989) at 1.465 GHz for Cul 0038-096. We follow Komissarov & Gubanov (1994) in using both flux measurements separately, assigning indices 'a' and 'b' to the different spectra. However, we note that Bagchi et al. (1998) and the relic flux density measure from the NVSS are in agreement with Slee & Reynolds (1984). We also fit our models to the radio spectrum of the relic source 1253+275. The relic is somewhat different to the six others in that it is rather extended and shows practically no break in its radio spectrum. Because of these differences, 1253+275 may have had a completely different origin and/or history compared to the other relics. However, we will show below that the radio spectrum of this source is also well fitted by our models. The radio fluxes for 1253+275 at seven radio frequencies can be found in Giovannini et al. (1991)

We fit the spectra adopting the fixed model parameters of the fiducial model and using t, t_s and p_s as free parameters. The goodness of the fit is determined by the standard χ^2-technique. The normalisation of the spectrum, A_f, is chosen such that for each set of free parameters the χ^2-value is minimised. The minimum of χ^2 as a function of the free parameters is found using a downhill simplex method in three dimension (e.g. Press et al., 1992). To avoid solutions with excessively young or old sources, we restricted t to the interval from 5×10^6 years to 5×10^8 years.

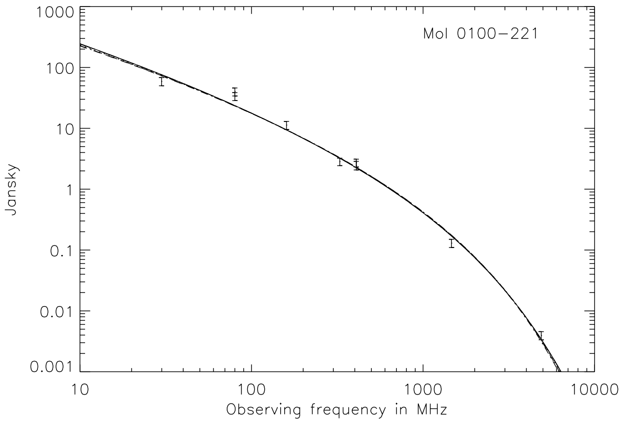

Figure 5. Model fits to the observed spectrum of Mol 0100-221. Subscripts 'JP' denote models with efficient pitch-angle scattering, subscripts 'KP' are assigned to models without pitch-angle scattering. Flux measurements are shown with their errors. Dotted line: Model $\mathrm{A_{JP}}$. Short-dashed line: Model $\mathrm{B_{JP}}$. Dash-dotted line: Model $\mathrm{C_{JP}}$. Dash-triple dotted line: Model $\mathrm{A_{KP}}$. Long-dashed line: Model $\mathrm{B_{KP}}$. Solid line: Model $\mathrm{C_{KP}}$.

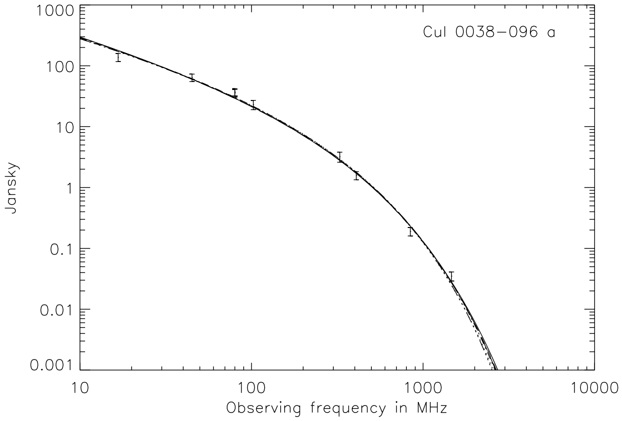

Figure 6. Same as Figure 5 but for Cul 0038-096 using flux measurement of Slee & Reynolds (1984) at 1.465 GHz.

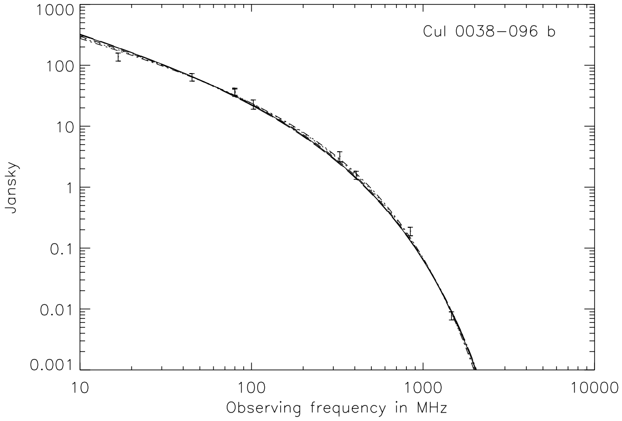

Figure 7. Same as Figure 5 but for Cul 0038-096 using flux measurement of Slee et al. (1989) at 1.465 GHz.

Table 2. Best fitting model parameters. The Abell number of the host cluster of the respective radio relic is given below the source name. Subscripts ‘JP’ denote models with efficient pitch-angle scattering, subscripts ‘KP’ are assigned to models without pitch-angle scattering.

		t / 10^6 years	t_s / 10^6 years	p_s / 10^{-13} ergs cm^{-3}	Q_j / 10^{44} ergs s^{-1}	$\rho_0 a_0^\beta$ / 10^7 g cm$^{-1.5}$	χ^2 / DOF
Mol 0100-221 A133	Model A_{JP}	167	139	90.3	2.6	187	6.13/6
	Model A_{KP}	41	34	2330	0.71	799	5.91/6
	Model B_{JP}	176	142	67.9	3.3	133	6.17/6
	Model B_{KP}	50	42	1654	0.81	764	5.92/6
	Model C_{JP}	165	136	90.8	1.8	193	6.20/6
	Model C_{KP}	37	32	3040	0.47	993	5.91/6
Cul 0038-096 a A85	Model A_{JP}	237	102	2.45	140	0.808	2.80/6
	Model A_{KP}	490	118	11.1	90	6.69	3.13/6
	Model B_{JP}	220	123	0.388	440	0.110	2.49/6
	Model B_{KP}	185	37	92.3	99	9.26	3.27/6
	Model C_{JP}	171	75	34.9	5.8	17.3	3.13/6
	Model C_{KP}	7.3	3.1	9160	1.2	43.0	3.07/6
Cul 0038-096 b A85	Model A_{JP}	153	31	2.03	1900	0.0467	2.26/6
	Model A_{KP}	496	99	13.9	140	5.84	4.29/6
	Model B_{JP}	171	41	3.95	840	0.199	3.12/6
	Model B_{KP}	499	111	13.1	160	6.63	4.64/6
	Model C_{JP}	259	55	0.874	160	0.0766	1.77/6
	Model C_{KP}	500	142	21.9	5.14	33.5	3.95/6
4C 38.39 A1914	Model A_{JP}	5.3	5.2	2.40×10^5	2.6	4430	3.05/6
	Model A_{KP}	130	130	9.84×10^4	1.3	6.51×10^5	2.53/6
	Model B_{JP}	440	383	44.7	17	387	4.67/6
	Model B_{KP}	499	494	4470	2.0	1.90×10^5	2.67/6
	Model C_{JP}	27	26	5.18×10^4	2.9	1.4×10^4	2.89/6
	Model C_{KP}	5.1	5.1	2.91×10^7	0.61	1.48×10^6	2.48/6
4C 63.10 A566	Model A_{JP}	63	61	4920	1.2	5020	2.18/5
	Model A_{KP}	56	55	2.73×10^4	0.44	3.55×10^4	2.08/5
	Model B_{JP}	29	28	1.14×10^4	1.1	3270	2.20/5
	Model B_{KP}	128	124	7740	0.53	3.59×10^4	2.08/5
	Model C_{JP}	5.2	5.0	1.07×10^5	0.78	2000	2.22/5
	Model C_{KP}	5.0	4.3	7.49×10^4	0.51	1080	2.80/5
3C 318.1 A2063	Model A_{JP}	198	141	73.2	6.2	130	1.37/11
	Model A_{KP}	106	73	533	2.4	459	1.35/11
	Model B_{JP}	203	142	64.6	7.4	110	1.37/11
	Model B_{KP}	27	17	2910	2.6	239	1.34/11
	Model C_{JP}	245	186	65.7	3.0	215	1.36/11
	Model C_{KP}	52	38	1650	0.91	627	1.34/11
3C 464 A2626	Model A_{JP}	429	382	84.2	1.8	1180	3.80/11
	Model A_{KP}	5.0	3.8	4.38×10^4	0.62	447	4.48/11
	Model B_{JP}	9.7	9.2	4.06×10^4	0.60	2040	3.27/11
	Model B_{KP}	5.0	4.1	6.36×10^4	0.48	830	4.02/11
	Model C_{JP}	25	24	2.87×10^4	0.51	8340	2.99/11
	Model C_{KP}	5.0	4.8	5.64×10^5	0.17	1.68×10^4	2.85/11
1253+275 Coma	Model A_{JP}	488	475	31.3	0.062	1010	3.57/4
	Model A_{KP}	249	248	2.47×10^5	0.0074	1.01×10^6	3.25/4
	Model B_{JP}	493	481	33.0	0.061	1100	3.56/4
	Model B_{KP}	5.02	5.01	7.82×10^5	0.0050	4.71×10^4	3.29/4
	Model C_{JP}	498	489	54.6	0.048	2040	3.49/4
	Model C_{KP}	5.38	5.38	5.86×10^6	0.0037	5.90×10^5	3.25/4

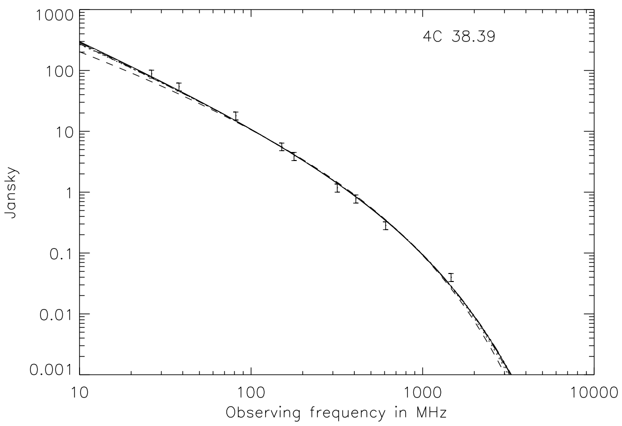

Figure 8. Same as Figure 5 but for 4C 38.39.

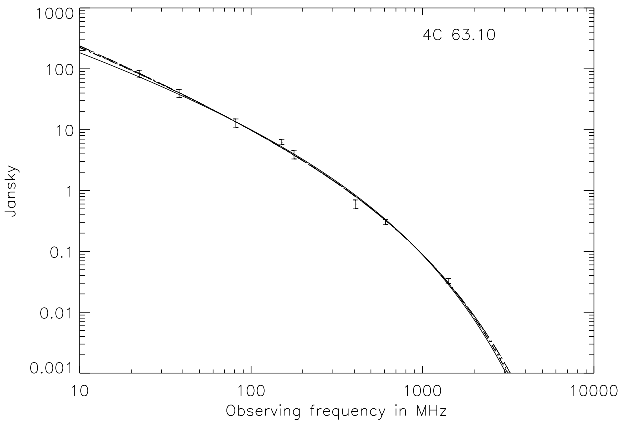

Figure 9. Same as Figure 5 but for 4C 63.10.

The best-fitting model parameters are summarised in table 2 and the resulting spectra are plotted in figures 5 through 11. In practically all cases the best-fitting spectra from the various models are almost indistinguishable from each other. In the following we briefly discuss the results for each source individually.

Mol 0100-221: The spectrum is well fitted by all models (reduced χ^2 between 0.99 and 1.03). The JP and KP-type models give somewhat different results for the free model parameters. However, within each family of models they are roughly consistent with each other. This indicates that the shape of the spectrum is mainly determined during the active phase of the source. The exact behaviour of the cocoon in the subsequent coasting phase has little influence. The JP-type models prefer older ages, higher jet powers and less dense environments compared to the KP-type models. KP-type models are marginally preferred over JP-type models.

Cul 0038-096: Both variants of the source spectrum can be successfully fitted by the models. However, the goodness of fit and the values of the free parameters vary significantly for each variant. The best fit achieved has a reduced χ^2-value of only 0.3, but predicts a very low density of the external gas. Three of the bets-fitting models (A_{KP} for variant a, A_{KP} and B_{KP} for variant b) have ages very close to the maximum age, $t = 5 \times 10^8$ years, allowed for the fit. At least for models A and B the JP-type and KP-type models give similar results, but models C are quite different from these.

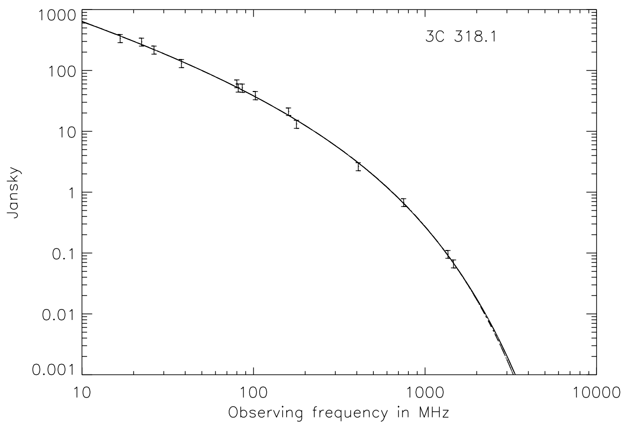

Figure 10. Same as Figure 5 but for 3C 318.1.

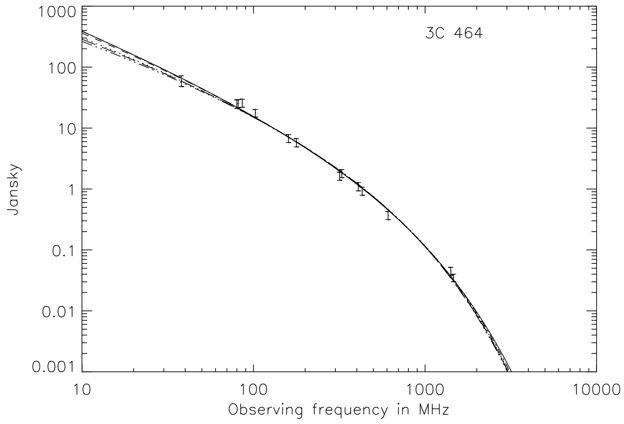

Figure 11. Same as Figure 5 but for 3C 464.

The spectrum of this source can be fitted reasonably well with all the models discussed here. However, a clear trend for the model parameters is not apparent.

4C 38.39: For this source models with high external densities are clearly preferred. However, the spread in the value of $\rho_0 a_0^{\beta}$ is considerable. There is also no agreement between the models with respect to the source age. From figure 8 it seems that the rather flat spectral break at high frequencies causes problems for all models. Again there is no discernible trend in the best-fitting parameters.

4C 63.10: The spectrum of this source is fitted about equally well by all models. In terms of the jet power, $Q_{\rm j}$, and the external density parameter, $\rho_0 a_0^{\beta}$, JP and KP-type models agree well with each other for models A and B, but there is a large range for the predicted source age. Models C require a somewhat lower density and they predict very low source ages.

3C 318.1: The model fits to the spectrum are very good with a reduced χ^2 of around 0.12. Values for $Q_{\rm j}$ and $\rho_0 a_0^{\beta}$ are similar for all models but again for this source there is a large spread for the source age.

3C 464: Except for model A_{JP}, all models predict rather low source ages. The best fits are achieved by both models C with rather high external densities. The predicted values of $Q_{\rm j}$ are fairly uniform but the external density vary strongly between models.

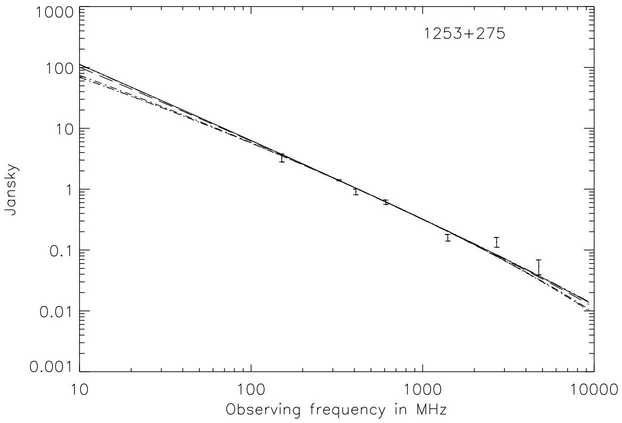

Figure 12. Same as Figure 5 but for 1253+275.

1253+275: The model parameters agree with each other for KP-type and JP-type models. However, the parameters are inconsistent between the two groups. The KP-type models prefer a young source age with virtually no influence of the phase in the source evolution when the jets are switched off. The predicted densities and pressures are very high. In the absence of radiative energy losses,our choice of $p = 2.5$ for the power law exponent of the energy distribution of the relativistic electrons at injection time, implies a spectral index of about -0.75. The observed spectrum of 1253+275 shows a spectral index of around -1.1 with no spectral break. The in general flatter spectra resulting from the KP-type models do not fit this steep spectrum well. Therefore, the model requires high external densities causing high pressure inside the lobes which subsequently show substantial energy losses and steeper spectra. The predictions of the JP-type model for an old source with moderate pressure values are more realistic. The low jet powers predicted by all models are caused by the substantially lower radio flux of this relic compared to the other sources.

5 CONCLUSIONS

We have developed a model for the evolution of the lobes of radio galaxies and radio-loud quasars of type FRII after the jets of the central AGN have stopped supplying them with energy. In the case that the lobes are still overpressured with respect to their surroundings, we show that their volume is proportional to

$$V \propto \begin{cases} t^{\frac{6(\gamma_{\rm c}+1)}{\gamma_{\rm c}(7+3\gamma_{\rm c}-2\beta)}} & ;\text{for } \gamma_{\rm c}=\gamma_{\rm s}, \\ t^{\frac{6}{2-\beta+3\gamma_{\rm c}}} & ;\text{for } \gamma_{\rm c}=4/3 \text{ and } \gamma_{\rm s}=5/3. \end{cases} \tag{9}$$

The proportionality given above for $\gamma_{\rm c}=\gamma_{\rm s}$ is, strictly speaking, not a solution of the equations governing the hydrodynamics. However, we have shown that is provides an excellent fit for the numerically found correct solution. The numerical calculations also show that the transition from the active phase with jets to the coasting phase without jets is fast.

We identify the lobes in the coasting phase with radio relic sources. The calculated model spectra depend only on a small number of source and environment parameters: The total age of the source, t, the age of the source when the jets were switched off, $t_{\rm s}$, and the pressure inside the lobes at that time, $p_{\rm s}$. We consider three limiting cases for the lobe evolution: The lobes continue to expand as if the jets were still supplying energy (Model A), the lobes continue to expand but with the modified dynamics found for the coasting phase and summarised above (Model B) and the lobes come into pressure equilibrium at the time the jets switch off and stop expanding (Model C). We also investigate the effects of efficient pitch-angle scattering (JP-type models) and its absence (KP-type models).

All our models can provide satisfactory to excellent fits to the observed spectra of radio relics. Taking into account the evolution of the strength of the magnetic field inside the lobe during the injection of relativistic electrons flattens the spectra sufficiently to explain the observations. Thus we cannot rule out efficient pitch-angle scattering as suggested by Komissarov & Gubanov (1994). Unfortunately, the good fits provided by all models also imply that the radio spectra of relic sources alone do not constrain any of the important source or environment parameters. The situation is aggravated by the findings of Slee et al. (2001) that the spectra can also be fitted using the alternative assumption of inhomogeneous magnetic fields inside the relics. Furthermore, even the inactive lobes may be re-ignited by compression during cluster mergers (Enßlin & Gopal-Krishna, 2001). Note here that the model of Enßlin & Gopal-Krishna (2001) for radio relics does not require the radio plasma to originate in a powerful FRII-type radio galaxy.

The morphologies of radio relics are very varied and only rarely resemble the well-defined lobes of active radio galaxies. This strongly suggests that fluid flows in the clusters significantly influence the evolution of radio galaxy remnants. Any re-acceleration or energisation due to compression would make it even more difficult to determine the original conditions in the relic. A possible solution could be the combination of radio spectra with X-ray observations of sufficient spatial resolution to identify inverse Compton scattered photons originating in the relativistic plasma of the relics. The X-ray observations could then be used to estimate the electron density while the radio emission would constrain the strength of the magnetic field. Despite the problems, it is interesting to note that our simple models can fit the radio spectra of all relic sources studied here. This includes the clearly curved spectrum of Cul 0038-096, a relic with substantial substructure, as well as the spectrum of 1253+275 without any significant spectral break and a comparatively smooth appearance. This would imply that, whatever the history of the relic source, even a rather simplistic model can explain the observed spectra in a variety of different ways thus making it impossible to constrain the conditions within the relic sources. We cannot rule out a complex history or re-acceleration of relativistic electrons influencing the properties of the relic sources. However, in the light of our results, such more complicated models are not required to fit the available radio data.

The degeneracy of model parameters can, however, also be turned to advantage in the case of statistical studies of the radio source population. For example, we can use the known radio luminosity function of active FRII objects and make predictions for the cosmological distribution of their remnants. Because of the mentioned degeneracy, these predictions will be almost model-independent. Such statistical studies can be used to predict the detection rate of radio galaxy remnants in low frequency radio surveys with high surface brightness sensitivity (Cotter & Kaiser, in preparation).

In fact, it is not yet clear whether radio relic sources are actually the remains of the lobes of powerful radio galaxies. Deep observations of radio galaxies in which the jet flows have stopped comparatively recently are necessary to decide whether the conditions inside their lobes point towards them evolving into relics (e.g. Kaiser et al., 2000). Clearly, the radio relic sources continue to challenge our understanding of the physics of radio galaxies and clusters.

ACKNOWLEDGMENTS

We would like to thank the anonymous referee for many helpful suggestions.

References

Bagchi J., Pislar V., Lima Neto G. B., 1998, MNRAS, 296, L23

Baldwin J. E., 1982, in Heeschen D. S., Wade C. M., eds, Extragalactic radio sources Evolutionary tracks of extended radio sources. Reidel, Dordrecht, p. 21

Brüggen M., Kaiser C. R., 2001, MNRAS, 325, 676

Churazov E., Brüggen M., Kaiser C. R., Böhringer H., Forman W., 2001, ApJ, 554, 261

Eilek J. A., Melrose D. B., Walker M. A., 1997, ApJ, 483, 282

Enßlin T. A., Gopal-Krishna 2001, A&A, 366, 26

Falle S. A. E. G., 1991, MNRAS, 250, 581

Fanaroff B. L., Riley J. M., 1974, MNRAS, 167, 31

Giovannini G., Feretti L., 2000, New Astron., 5, 335

Giovannini G., Feretti L., Stanghellini C., 1991, A&A, 252, 528

Giovannini G., Tordi M., Feretti L., 1999, New Astron., 4, 141

Goldshmidt O., Rephaeli Y., 1994, ApJ, 431, 586

Govoni F., Feretti L., Giovannini G., Böhringer H., Reiprich T. H., Murgia M., 2001, A&A, 376, 803

Gull S. F., Northover K. J. E., 1973, Nat., 224, 80

Jaffe W. J., Perola G. C., 1973, A&A, 26, 423

Kaiser C. R., 2000, A&A, 362, 447

Kaiser C. R., Alexander P., 1997, MNRAS, 286, 215

Kaiser C. R., Dennett-Thorpe J., Alexander P., 1997, MNRAS, 292, 723

Kaiser C. R., Schoenmakers A. P., Röttgering H. J. A., 2000, MNRAS, 315, 381

Kardashev N. S., 1962, SvA, 6, 317

Kempner J. C., Sarazin C. L., 2001, ApJ, 548, 639

Komissarov S. S., Gubanov A. G., 1994, A&A, 285, 27

Landau L. D., Lifshitz E. M., 1987, Fluid mechanics, 2nd edition. Butterworth-Heinemann, Oxford

Leahy J. P., 1991, in Hughes P. A., ed., Beams and jets in astrophysics Interpretation of large scale extragalactic jets. Cambridge University Press, p. 100

Pacholczyk A. G., 1970, Radio Astrophysics. Freeman, San Francisco

Press W. H., Teukolsky S. A., Vetterling W. T., Flannery B. P., 1992, Numerical Recipes. Second edition.. Cambridge University Press, Cambridge, UK.

Reynolds C. S., Begelman M. C., 1997, ApJ, 487, L135

Reynolds C. S., Heinz S., Begelman M. C., 2001, ApJ, 549, L179

Sedov L. I., 1959, Similarity and dimensional methods in mechanics.. Academic Press, London

Slee O. B., Perley R. A., Siegman B. C., 1989, Austral. J. Phys., 42, 633

Slee O. B., Reynolds J. E., 1984, Proc. Astron. Soc. Aust., 5, 516

Slee O. B., Roy A. L., Murgia M., Andernach H., Ehle M., 2001, AJ, 122, 1172

Tribble P. C., 1994, MNRAS, 261, 57